Taylor & Francis
Taylor & Francis Group

Australian Journal of Earth Sciences

An International Geoscience Journal of the Geological Society of Australia

ISSN: 0812-0099 (Print) 1440-0952 (Online) Journal homepage: www.tandfonline.com/journals/taje20

The geochemistry of Ga, Ge and In in magmatic–hydrothermal tin–polymetallic deposits of the Herberton Mineral Field, Australia

A. Kumar, I. Sanislav & M. Sami

To cite this article: A. Kumar, I. Sanislav & M. Sami (17 May 2026): The geochemistry of Ga, Ge and In in magmatic–hydrothermal tin–polymetallic deposits of the Herberton Mineral Field, Australia, Australian Journal of Earth Sciences, DOI: 10.1080/08120099.2026.2661994

To link to this article: https://doi.org/10.1080/08120099.2026.2661994

AUSTRALIAN JOURNAL OF EARTH SCIENCES
https://doi.org/10.1080/08120099.2026.2661994

The geochemistry of Ga, Ge and In in magmatic–hydrothermal tin–polymetallic deposits of the Herberton Mineral Field, Australia

A. Kumar[a], I. Sanislav[a] and M. Sami[b]

[a]Economic Geology Research Centre (EGRU), Department of Earth and Environmental Sciences, James Cook University, Townsville, Australia; [b]Geosciences Department, College of Science, United Arab Emirates University, Al Ain, United Arab Emirates

ABSTRACT

The geochemistry of In, Ga and Ge of muscovite and topaz was investigated from magmatic–hydrothermal systems related to tin and polymetallic vein mineralisation associated with Carboniferous–Permian granites from the Herberton Mineral Field (HMF) in northeast Queensland. Muscovite and topaz from the Baal Gammon and Isabel deposits were sampled and analysed. Each deposit shows two stages of hypogene mineralisation. The first stage is related to tin mineralisation associated with reduced intrusive rocks including the Jumna Granite, the Herberton Hill Granite and the UNA Porphyry. The second stage is related to Cu mineralisation associated with oxidised magmas that formed during the emplacement of the Slaughter Yard Creek Volcanics. Muscovite and topaz associated with the reduced intrusive rocks mainly occur in the greisen derived from the UNA Porphyry, whereas the muscovite associated with the oxidised phase occur with the massive sulfide mineral assemblage hosted by the Slaughter Yard Creek Volcanics and the Hodgkinson Formation. In general, the topaz grains have higher concentrations of Ga and Ge (average 196 ppm and 68 ppm, respectively) than the muscovite grains (average Ga = 8.4 ppm and Ge = 2 ppm). In contrast, muscovite grains have higher In concentrations (up to 60 ppm) than the topaz grains (below limit of detection). The normalised trace-element pattern of muscovite grains from different tin deposits indicates that Ga and Ge have a negative anomaly in oxidised granites and a positive anomaly in reduced granites. In contrast, the In anomaly is not sensitive to the oxidation state of the magmas. Geochemical modelling indicates that In forms stable complexes in acidic conditions, whereas Ga and Ge form stable complexes with oxide and hydroxide ions in near-neutral to weakly basic and reduced conditions. Thus, the geochemistry of In is decoupled from that of Ga and Ge owing to the redox conditions of the magmatic–hydrothermal systems.

KEY POINTS

1. An improved understanding of the geochemistry of Ga, Ge and In in magmatic–hydrothermal systems of polymetallic tin deposits.
2. Gallium, Ge and In content in muscovite was identified to be influenced by the redox state of the granites.
3. Gallium and Ge uptake in muscovite was interpreted to be enhanced in reduced systems from a global muscovite dataset from tin fields.
4. Indium was identified to be amphoteric and susceptible to pH changes in hydrothermal systems.

ARTICLE HISTORY
Received 16 October 2025
Accepted 11 April 2026

KEYWORDS
semiconductor metals; indium; gallium; germanium; Herberton; Queensland

Introduction

Gallium and Ge are key metals used in the semiconductor industry for developing advanced electronic technologies (Lu *et al*., 2017; Moskalyk, 2004; Zheng *et al*., 2023), while In is used in flat panel displays, touchscreens and photovoltaic cells (Fontana *et al*., 2021; Frenzel *et al*., 2017; Watari *et al*., 2020). Indium, Ga and Ge are extracted as by-products from base-metal deposits (Frenzel *et al*., 2017; Huston & Bastrakov, 2024), which are mostly magmatic–hydrothermal in origin. The geochemical conditions that concentrate Ga, Ge and In in magmatic–hydrothermal systems are not well understood. In this research we used the alteration minerals muscovite and topaz trace-element content to explore the hydrothermal geochemistry of Ga–Ge–In. The geochemistry of muscovite and topaz effectively displays geochemical processes that occurred during the formation of ore deposits (Monnier *et al*., 2022; Peng *et al*., 2023; Soltani Dehnavi *et al*., 2018; Uribe-Mogollon & Maher, 2018). Muscovite has been used to track subtle variations in trace elements within mineral deposits that reflect physicochemical conditions of mineralising fluids (*e.g.* van Ryt *et al*., 2019). Muscovite can incorporate a wide range of elements in its structure, including Cs, K, Na, Rb, Ba, Li, Fe, Mg, Mn, Zn, Al, Cr, V and Ti (Rieder *et al*., 1999) and has been used as a vector in porphyry copper, volcanogenic massive

CONTACT A. Kumar avish.kumar@jcu.edu.au Economic Geology Research Centre (EGRU), Department of Earth and Environmental Sciences, James Cook University, Townsville, Australia

Supplemental data for this article can be accessed online at https://doi.org/10.1080/08120099.2026.2661994.
Editorial handling: Anita Andrew

sulfide (VMS) and rare metal granite deposits. Muscovite from oxidised porphyry sources shows systematic variation in V, Ti, B, Co, Cs, Mn, Tl, Li, Sn and Sr (Uribe-Mogollon & Maher, 2018), while muscovite from reduced source in VMS deposits show spatial variation in Tl, As, Sb, Sn, Hg and In (Soltani Dehnavi *et al*., 2018). Muscovite minerals in Sn–W greisen and rare metal granite deposits of fractionated and reduced sources show variations in Sn, Nb, Ta, Cs, Li, Rb and W (Breiter *et al*., 2023; Codeço *et al*., 2021), but their geochemistry has not been compared with muscovite originating from oxidised rocks that intruded the parent pluton. Trace-element studies on hydrothermal topaz are limited, since it mostly occurs in highly fractionated granites (Soufi, 2021). Additionally, recognising hydrothermal topaz in hand specimens without analytical techniques can be challenging, since they have a similar appearance to hydrothermal quartz. Based on limited studies, topaz crystal structure appears to be a good host for Ga and Ge (Agangi *et al*., 2016; Breiter *et al*., 2013; Gauzzi *et al*., 2018; Gauzzi & Graça, 2018; Setkova *et al*., 2024). Gallium and Ge form stable complexes with oxide–hydroxide group ligands (Wood & Samson, 2006), whereas In complexes with chlorine (Kumar *et al*., 2023) in hydrothermal environment. Therefore, we used the Herberton Mineral Field (HMF), which hosts multiple tin deposits affected by a later oxidised intrusion, as a study site to investigate the behaviour of Ga–Ge–In in reduced and oxidised magmatic–hydrothermal environments by using muscovite and topaz trace-element geochemistry. Furthermore, muscovite geochemistry from oxidised sources at the HMF is compared with those from reduced sources in tin fields from the literature to evaluate the behaviour of Ga–Ge–In in magmatic–hydrothermal systems.

Zircon and whole-rock geochemistry was used to further confirm the petrogenesis of the source rocks of muscovite and topaz at the Baal Gammon and Isabel deposits in the HMF. The key objective of this study is to evaluate how Ga, Ge and In partitioning in hydrothermal minerals responds to contrasting fluid conditions associated with reduced *vs* oxidised magmatic systems. The HMF provides a unique natural laboratory where reduced tin-bearing granites are overprinted by younger oxidised magmatic units, allowing direct comparison of trace-element behaviour under distinct hydrothermal regimes within the same geological framework.

Geological background

The Mossman Orogen at the northern extremity of the Tasmanides, Queensland, Australia hosts the Sn–W deposits of the HMF (Figure 1). The HMF comprises multiple Sn–W together with polymetallic Au, Cu, Zn, Sn, W and Mo deposits (Blake, 1972) that occur throughout the Tasmanides. The Tasmanides consists of a series of orogenic belts that were initiated during the breakup of Rodinia, followed by the formation of Gondwana, the collision of Gondwana and Laurasia, and terminated during the breakup of Pangea (Cawood, 2005; Dirks *et al*., 2021; Edgar, Sanislav, & Dirks, 2022; Edgar, Sanislav, Dirks, *et al*., 2022; Glen, 2005; Klootwijk, 2013). The Tasmanides include the Delamerian, Thomson, Lachlan, Mossman and New England orogens (Figure 1a; Edgar *et al*., 2023; Rosenbaum, 2018).

The Sn–W deposits of the HMF occur in the eastern section of the Mossman Orogen, which consists of multiply deformed turbidite sequence of the Hodgkinson Formation (Figure 1b; Henderson *et al*., 2013; Withnall & Henderson, 2012). The source of these deposits is linked to the Kennedy Igneous Association (Figure 1b; Cheng *et al*., 2018; Kumar *et al*., 2022) that intrudes the Hodgkinson Formation. Two episodes of tin mineralisation at *ca* 337 Ma and *ca* 322 Ma are identified from zircon age compilations of units within the Kennedy Igneous Association (Kumar *et al*., 2022). These tin-bearing units form part of the O'Briens Creek Supersuite, which consists of highly fractionated granites that were emplaced between *ca* 365 and 317 Ma (Champion, 1991; Cheng *et al*., 2018; Kumar *et al*., 2022). A later episode of magmatism between 305 and 285 Ma formed the polymetallic Cu, Zn and In sulfide deposits at the Baal Gammon and Isabel deposits (Kumar *et al*., 2022). The intrusion of these oxidised magmas into the earlier reduced Sn-bearing system is particularly significant because it introduces a distinct hydrothermal environment characterised by different redox conditions and fluid compositions. This overprinting event generates a second stage of hydrothermal alteration, including muscovite associated with sulfide mineralisation, which contrasts with the earlier greisen and topaz assemblages formed from reduced fluids. As a result, muscovite formed during the oxidised stage provides a direct record of trace-element behaviour under contrasting fluid conditions, allowing evaluation of how Ga, Ge and In respond to changes in hydrothermal environment within the same geological system. These polymetallic sulfide-bearing units are part of the Koolmoon Volcanic Group (Figure 1b; *ca* 290 Ma; Kumar *et al*., 2022) in the eastern section, while the semi-equivalent unit in the western part is the Featherbed Volcanics.

Three stages of mineralisation are recognised in the HMF. The first stage is associated with Sn and early greisen formation (Kumar, Sanislav, Huang *et al*., 2024), the second to Cu, Zn, In and other sulfides, and the third to the development of a supergene profile. At the Baal Gammon deposit, Sn is hosted within the greisenised UNA Porphyry. Hydrothermal topaz associated with the Sn deposit occurs as veins and breccia infill surrounding the UNA Porphyry. At the Isabel deposit, the early Sn phase occurs as altered cassiterite in polymetallic Zn–In veins (Kumar, Sanislav, Martin *et al*., 2024). The second stage of mineralisation consists of Cu–In polymetallic veins at the Baal Gammon deposit and Zn–In polymetallic veins at the Isabel deposit (Kumar, Sanislav, Martin *et al*., 2024). The second stage of mineralisation formed hydrothermal muscovite, which occurs with sulfides in vein walls and in mineralised breccias (Kumar *et al*., 2022). The third stage consists of supergene alteration of the sulfide and occurs as Cu–Fe oxides and carbonates (Kumar, Sanislav, Martin *et al*., 2024).

Materials and methods

Samples

Eight samples were collected from the regional Herberton Hill Granite, 11 from Jumna Granite and five from the Slaughter Yard Creek Volcanics. Four samples were collected from the UNA

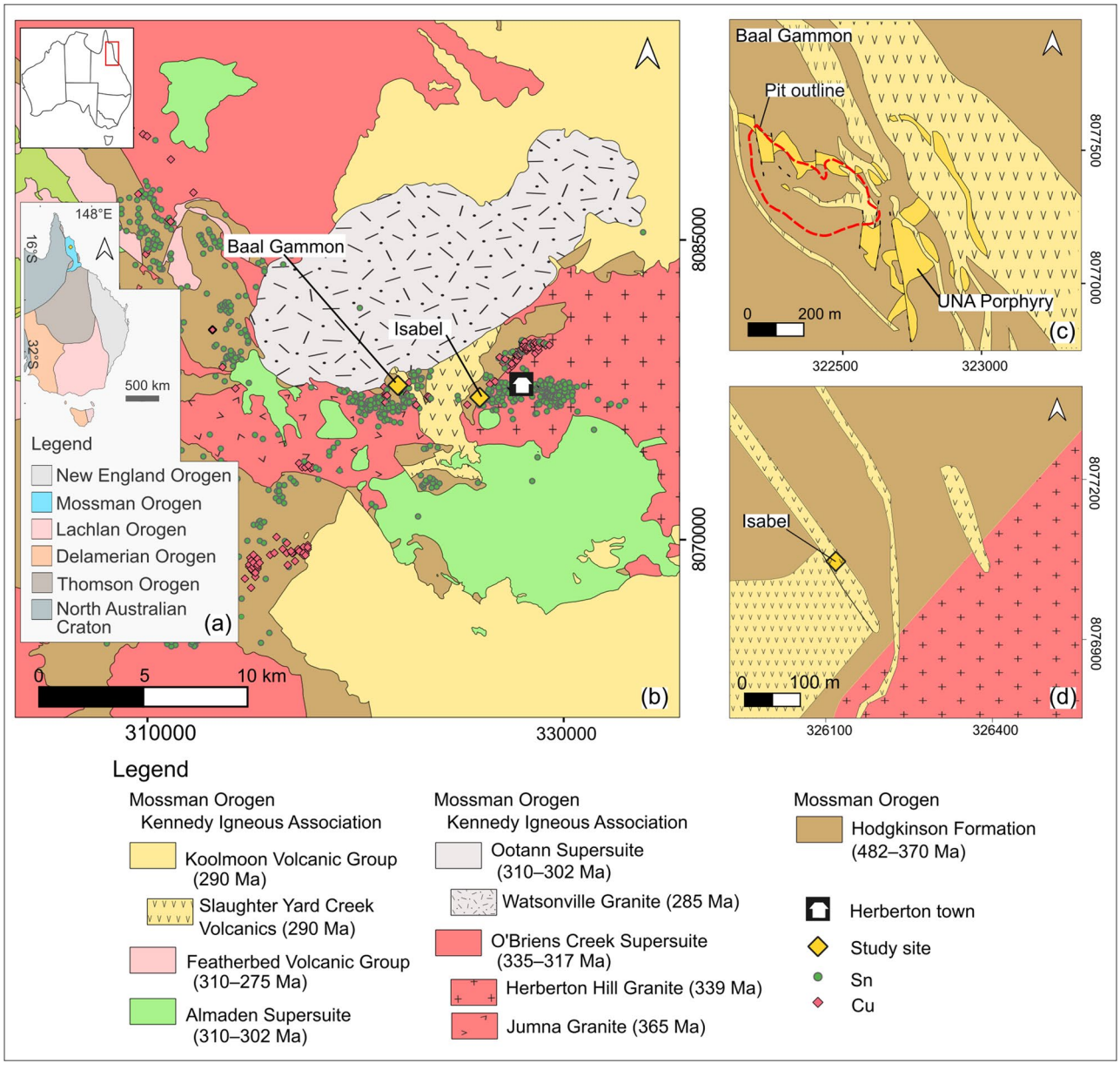

Figure 1. Simplified geological maps of: (a) orogens in East Australia; (b) the Herberton Mineral Field; (c) the Baal Gammon deposit; and (d) the Isabel deposit. The Slaughter Yard Creek Volcanics are oxidised, whereas the rocks within the O'Briens Creek Supersuite are reduced (Kumar, Sanislav, Cathey, *et al.*, 2023).

Porphyry at the Baal Gammon deposit and two samples from the Isabel deposit. Representative samples were selected for thin-sectioning and microscopic analyses from the regional granites (Figure 2), UNA Porphyry and the alteration zones in the Baal Gammon and Isabel deposits. Trace elements were analysed on topaz from reduced and altered UNA Porphyry (Figure 2d) and muscovite from the massive sulfides at the Baal Gammon deposit (Figure 2e) and muscovite from the hydrothermal breccia at the Isabel deposit linked with relatively oxidised Slaughter Yard Creek Volcanics.

Whole-rock geochemistry

Major oxides and trace-element concentrations were analysed by the Bureau Veritas Minerals, Vancouver with the ICP-OES/MS instrument (analytical package LF202). The whole-rock samples were digested with $LiBO_2/Li_2B_4O_7$ fusion for rare earth and refractory elements and aqua regia for mobile and soluble species. Iron oxide (FeO) was determined by titration (analytical package GC806). The trace-element and REE data were normalised against primitive mantle and chondrite values, respectively, from Palme and O'Neill (2014).

Mineral trace elements

Laser-ablation inductively coupled plasma mass spectrometry (LA-ICP-MS) was used for *in situ* trace-element analyses of muscovite and topaz from the ore assemblage at the Baal Gammon deposit, muscovite from the Isabel deposit and zircons from the regional granites and UNA Porphyry. Laser

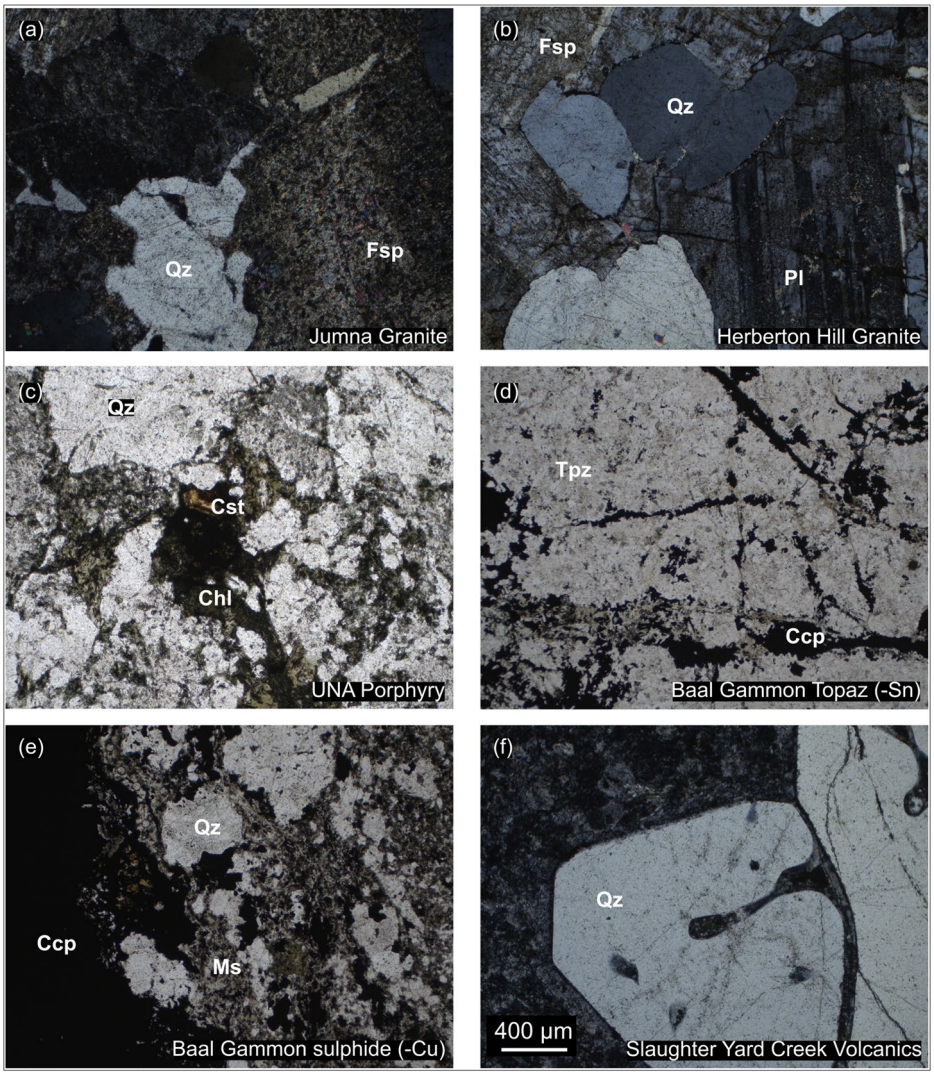

Figure 2. Photomicrograph of: (a) Jumna Granite showing quartz (Qz) with sericite-altered feldspar (Fsp); (b) Herberton Hill Granite with quartz, altered feldspar and plagioclase (Pl); (c) UNA Porphyry with cassiterite (Cst) and chlorite (Chl) alteration of mica; (d) topaz (Tpz) breccia in the UNA Porphyry; (e) massive sulfide vein wall from the Baal Gammon deposit showing muscovite and hydrothermal quartz; and (f) Slaughter Yard Creek Volcanics showing embayment texture in quartz. Scale bar applies to all photomicrographs.

analyses were performed using an Analyte G2 Excimer Laser Ablation system coupled to a Thermo iCap-TQ ICP-MS instrument at the Advanced Analytical Centre, James Cook University. Laser ablation was carried out with an energy density of 2 J/cm^2 at a rate of 5 Hz on a spot size of 50 µm for muscovite and topaz and 40 µm for zircon. The reference material NIST610 was used as an internal standard, and Si values fixed to mineral stoichiometry were used for data reduction to yield quantitative element concentrations. The standards NIST612, GSE-1 and GSD-1 were used as external standards for monitoring matrix effects. A mixture of helium and argon was used as the carrier gas for transporting the ablated analyte into the ICP-MS analysis chamber. The LA-ICP-MS trace-element data were reduced using Iolite software (Fisher *et al.*, 2017; Paton *et al.*, 2011), and the laser peaks were inspected for spikes to differentiate mineral inclusions. Trace-element results are included in the supplemental data, and a summary of the muscovite and topaz trace elements is provided in Table 1.

Geochemical modelling

Geochemical modelling of Ga and In complexes was conducted with The Geochemist's Workbench (GWB) Community Edition 13 (Bethke *et al.*, 2022) software to investigate the redox geochemistry of metal complexes over a range of Eh and pH. The ΔG_f and K_{eq} values for modelling were adopted from the Thermoddem database (Blanc *et al.*, 2012; Boschetti, 2023). Gallium, Ge and In were modelled at concentrations (10^{-6} M) similar to those observed in active hydrothermal systems at 300 °C and the ligands Cl^- and OH^- at 10^{-1} M (*e.g.* Seward *et al.*, 2014; Simmons *et al.*, 2016). The supplemental data include individual Ga, Ge and In plots (Appendix 4) and thermodynamic constraints (Appendix 5).

Results

Petrography

The felsic rocks from the HMF show equigranular, porphyritic, aphyric and hydrothermal textures. The tin granites including

Table 1. Summary of trace-element concentrations (ppm) in muscovite and topaz from the Baal Gammon and Isabel deposits.

Sample (n = 19)	BIN019		BIN025		BIN005		IN005	
Mineral	Muscovite		Muscovite		Topaz		Muscovite	
Deposit	Baal Gammon		Baal Gammon		Baal Gammon		Isabel	
Associated unit	Slaughter Yard Creek Volcanics		UNA Porphyry		UNA Porphyry		Slaughter Yard Creek Volcanics	
ppm	Mean	SD	Mean	SD	Mean	SD	Mean	SD
Mg	2760	608	2868	554	325	831	1093	236
K	74 566	8473	78 960	2902	240	247	59 338	1315
Mn	406	377	236	75	72	41	83	16
Fe	30 406	30 080	18 359	4128	2478	2190	4599	535
Cu	5891	8782	3.7	2.5			2.7	1.1
Zn	903	2113	89	24			232	80
Pb	487	780	30	27	1.1	1.3	9	4.5
In	60	69	5.5	1.0			0.8	0.2
Ga	68	10	106	23	8.4	1.3	39	2.0
Ge	2.1	1.0	2.2	0.5	196	27	0.4	0.2
Sr	52	9	5	1.7	3.9	1.9	9.2	2.8
Y	2.3	2.1	0.1	0.0	6.3	3.7	2.2	2.6
Nb	19	5	26	4.5	1.6	1.6	0.2	0.0
Cs	79	18	15	8.5	0.3	0.3	28	1.6
Ba	412	50	179	78	1.9	5.0	165	78
Ti	1016	135	1174	264	255	411	139	25

the Jumna Granite and Herberton Hill Granite consist of equigranular textures with weak to moderate alteration of the feldspar (Figure 2a, b). The Jumna Granite predominantly comprises 4–5 mm equigranular quartz and feldspars with polysynthetic twinning, whereas the Herberton Hill Granite consists of 4–5 mm quartz, 10–15 mm plagioclase and 10 mm K-feldspar with polysynthetic twinning (Figure 2). The feldspars in both granites have been altered to sericite, whereas most of the muscovite and biotite have been altered to chlorite. The tin-bearing UNA Porphyry consists of quartz, feldspar, chloritised muscovite, biotite and cassiterite (Figure 2c). The UNA Porphyry contains 1–2 m-thick zones of hydrothermal topaz that formed during Sn mineralisation (Figure 2d). The hydrothermal topaz has a brownish tinge and is weakly brecciated with sulfide infill (Figure 2d). Hydrothermal muscovite is intergrown with the sulfide mineral assemblage at the Baal Gammon and Isabel deposits (Figure 2e), which occur along the margins of massive sulfide and in incipient breccia of hydrothermal quartz set in a loose jigsaw-fit texture surrounding the massive sulfides (Figure 2e). The oxidised porphyritic rocks occur mostly within the Slaughter Yard Creek Volcanics group. Near the massive sulfide deposits, quartz crystals display embayment textures in porphyritic rocks (Figure 2f) that have sericite-altered aphanitic groundmass.

Whole-rock geochemistry

The Jumna Granite and Herberton Hill Granite have a SiO_2 content greater than 75 wt% (supplemental data, Appendix 1) with moderate variations in Al_2O_3 (8.4–13.2 wt%), MgO (0.03–0.12 wt%), Na_2O (0.09–3.26 wt%) and CaO (0–0.65 wt%). The Slaughter Yard Creek Volcanics contain noticeable variations in SiO_2 (71–76 wt%), Al_2O_3 (12.4–14 wt%), MgO (0.09–0.67 wt%), Na_2O (3.09–3.7 wt%) and CaO (0.4–1.88 wt%). The whole-rock geochemistry data were plotted on Shand's (1948) classification diagram (Figure 3) with all the felsic rock units plotting in the peraluminous field, except for one sample of the Slaughter Yard Creek Volcanics, which plots in the metaluminous field (Figure 3a). The Herberton Hill Granite, Jumna Granite and the UNA Porphyry plot in the differentiated field (Figure 3b) on the Ba–Rb–Sr ternary diagram of El Bouseily and El Sokkary (1975) and have A-type affinities (Figure 3c) on the Zr *vs* 10 000 Ga/Al plot of Whalen *et al*. (1987). The Slaughter Yard Creek Volcanics contain lower Nb and Y concentrations (Figure 3d) and plot in the I-type field on the Zr *vs* 10 000 Ga/Al diagram.

The UNA Porphyry also contains significant variations in its major-element concentrations (supplemental data, Appendix 1). All the felsic units have a similar normalised trace-element pattern on the spider diagram (Figure 3e) and display negative anomalies for Ba, Nb, Sr and Ti. The normalised REE plot of these units has a higher negative Eu anomaly for differentiated granites, including the Herberton Hill Granite, the Jumna Granite and the UNA Porphyry, than the Slaughter Yard Creek Volcanics (Figure 3f).

Mineral chemistry

Zircon

The normalised REE patterns of the zircon from all the felsic units are similar (Figure 4a). The Herberton Hill Granite and the Slaughter Yard Creek Volcanics have the lowest total REE + Y with averages at 3301 ppm and 4111 ppm, respectively. The Jumna Granite (average 13 314 ppm) and the UNA Porphyry (average 7563 ppm) contain the highest average for total REE + Y (Figure 4b). Similar patterns were observed for P concentrations, with lower averages in zircons from the Herberton Hill Granite (average 591 ppm) and the Slaughter Yard Creek Volcanics (average 531 ppm) and higher averages in the Jumna Granite (average 1756 ppm) and the UNA Porphyry (average 1590 ppm). The UNA Porphyry (average 7.7 ppm) and the Slaughter Yard Creek Volcanics (average 6.7 ppm) have low averages for Ti concentrations. A high average Ti concentration is present in zircon from the Jumna Granite (average 38 ppm). The zircon trace elements show a systematic increase in U, Th, Ta, Nb, Y, P, Fe and Sn (Figure 4c–f) from the Slaughter Yard Creek Volcanics to the Herberton Hill Granite, to the UNA Porphyry and the Jumna Granite. Zircon trace-element results are provided in the supplemental data (Appendix 2).

Muscovite and topaz

The trace-element variations in muscovite grains from the UNA Porphyry, the Baal Gammon massive sulfides and the Isabel hydrothermal breccia are similar (Figure 5), except for Nb. The Isabel muscovite contains low concentration of Nb (average 0.2 ppm; Table 1). The Baal Gammon muscovite contains higher concentrations of Cu, Zn, Pb and Fe, which may indicate sulfide inclusions that could not be avoided during the analysis. Therefore, Cu, Zn, Pb and Fe have a higher standard deviation than other elements (Table 1). The Baal Gammon topaz contains low concentrations of Ba, Mg, Ti, Cs and Na compared with the muscovite grains (Figure 5). The average concentrations of Ge

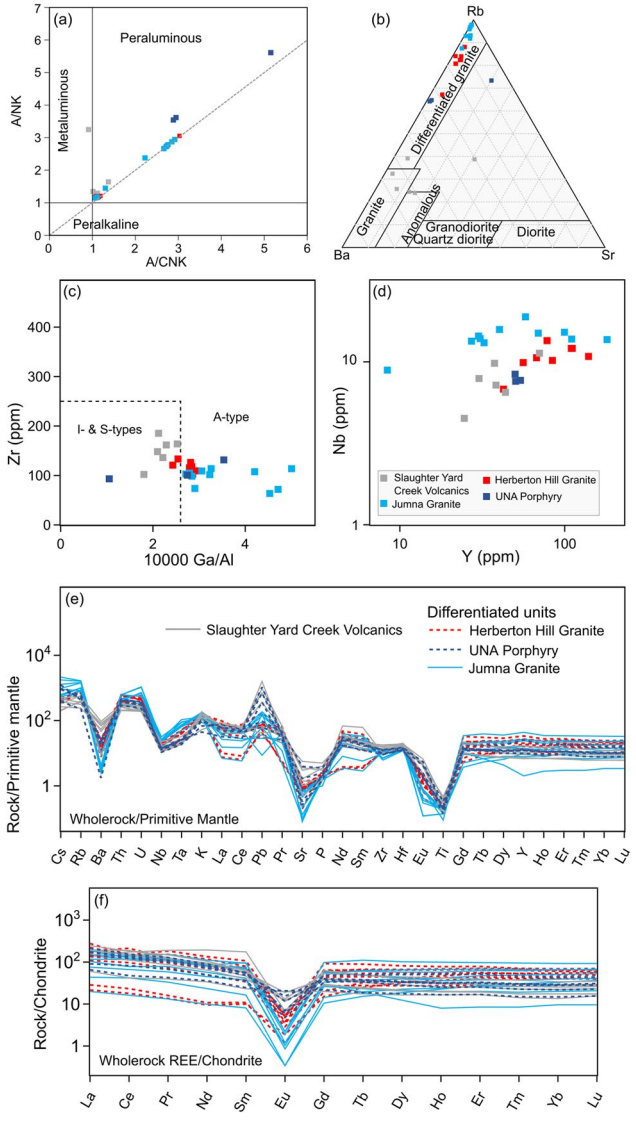

Figure 3. Geochemical classification (a–d), spider plot (e) and REE (f) plot of the Herberton Mineral Field granites. (a) A/NK *vs* A/CNK plot of Shand (1948), showing aluminium saturation for the HMF rocks. (b) Rb–Ba–Sr ternary diagram of El Bouseily and El Sokkary (1975) showing differentiated and normal granites. (c) Zr *vs* 10 000 Ga/Al diagram with I-, S- and A-type fields for granites adopted from Whalen *et al*. (1987). (d) Y *vs* Nb variation plot. (e) Primitive mantle (values from Palme & O'Neill, 2014) normalised spider plot. (f) Chondrite (values from Palme & O'Neill, 2014) normalised REE distribution pattern.

and Ga in topaz are 196 ppm and 60 ppm, respectively, whereas in muscovite, the average concentrations are 2 ppm for Ge and 8.4 ppm for Ga. The Baal Gammon and Isabel muscovite contains variable In (0.83–60 ppm) concentrations. The In concentration in topaz was below the limit of detection. Muscovite and topaz trace-element results are provided in the supplemental data (Appendix 3).

Eh, pH estimates for In and Ga complexes

The result of geochemical modelling is presented in Figure 6 as an Eh *vs* pH plot. The plot indicates that $InCl^{2+}$ complex is favoured in low pH (~2), while InO_2^- and $Ga(OH)_4^-$ are formed in neutral to high pH (~6) and reduced conditions at 300 °C. The modelling shows that between pH 2 and 6, the aqueous species $HInO_2$ may also occur.

Discussion

Magmatic and magmatic–hydrothermal evolution of the reduced tin-bearing granites and the oxidised volcanics from the HMF

The alteration mineralogy (Figure 2d–f), whole-rock geochemistry (Figure 3) and zircon trace-element content (Figure 4; supplemental data, Appendix 2) of the Sn-bearing granites from the HMF can be used to examine their magmatic and magmatic–hydrothermal history. The tin-bearing granites in the HMF belong to the O'Briens Creek Supersuite, and near the Baal Gammon deposit they include the Herberton Hill Granite and the Jumna Granite. The youngest magmatic episode of Sn mineralisation was constrained by zircon geochronology at 333 Ma (Kumar *et al*., 2022), which is older than the cassiterite mineralisation age of 318 Ma (Cheng *et al*., 2019). The granites in the O'Briens Creek Supersuite have been classified as I-type by Champion and Chappell (1992), where highly fractioned I-type granites show an A-type character with elevated Ga, Nb and Y concentrations. The Herberton Hill Granite and Jumna Granite contain high Ga, Nb and Y (Figure 3d), which confirms the A-type character. The Herberton Hill Granite, Jumna Granite and the UNA Porphyry are high in silica (>75 wt%; Figure 3), Rb and Sr, exhibit large negative Eu anomalies (Figure 3f) and therefore are highly differentiated (Figure 3b; Cheng *et al*., 2018; Kumar, Sanislav, Martin *et al*., 2024), which is typical for tin-bearing granites (Zhang *et al*., 2019). The Fe_2O_3/FeO *vs* Rb/Sr plot of Blevin and Chappell (1995) indicates that the O'Briens Creek Supersuite formed from a reduced magma (Figure 7), which was expected, as tin deposits worldwide are associated with reduced magmas and hydrothermal fluids (Eugster, 1985; Ishihara, 1981; Sillitoe & Lehmann, 2022). Our data indicate that some of the units, including the UNA Porphyry, Jumna Granite and Herberton Hill Granite within the O'Briens Creek Supersuite, express an oxidised signature on the Fe_2O_3/FeO *vs* Rb/Sr plot (Figure 7) but still preserve a large negative Eu anomaly typical of tin granites. This may suggest that the O'Briens Creek Supersuite was contaminated during the intrusion of oxidised units such as the Slaughter Yard Creek Volcanics.

At the Baal Gammon deposit, the UNA Porphyry, which hosts a tin deposit, exhibits similar whole-rock geochemical signatures to those of the Herberton Hill Granite and Jumna Granite (Figure 3). However, the UNA Porphyry was dated at 333 Ma and contains a population of zircon ages at 363 Ma, and based on the spatial relationship and the inherited zircon population, it was interpreted to be derived from the same sources as the Jumna Granite, which was emplaced at 365 Ma (Kumar *et al*., 2022). Furthermore, the zircon REE+Y and P binary plot (Figure 4b) indicates that the Jumna Granite and the UNA Porphyry zircon contain high P (average 1756 and 1590 ppm, respectively) compared with the Herberton Hill Granite (average 590 ppm) that is likely due to the inheritance of the UNA Porphyry from the Jumna Granite. The higher U, Th, Nb, Ta, Y, P, Fe and Sn (Figure 4) content in zircon from the Jumna Granite and UNA Porphyry further suggests that they may have

formed from a more evolved melt (Duan *et al.*, 2024) than the Herberton Hill Granite. The Sn magmatism in the HMF is composed of reduced magmas enriched in F (Cheng *et al.*, 2018), which allowed extreme levels of fractionation and formed topaz, fluorite, white mica and in places tourmaline as alteration minerals during its hydrothermal activity (Blake & Smith, 1971; Kumar *et al.*, 2022).

The oxidised volcanics of the HMF are younger than the Sn-bearing granites at the HMF, and they belong to the Koolmoon Volcanic Group and other units of similar age (*ca* 290 Ma) within the Kennedy Igneous Association (Kumar *et al.*, 2022). The field relationships indicate that these oxidised volcanic rocks crosscut the tin-bearing granites and formed small to medium-sized sulfide deposits (Kumar, Sanislav, Martin *et al.*, 2024). At the Baal Gammon and Isabel deposits, the Slaughter Yard Creek Volcanics of the Koolmoon Volcanic Group was dated at 290 Ma (Kumar *et al.*, 2022). The Slaughter Yard Creek Volcanics have an I-type affinity and are weakly peraluminous (Figure 3), which is typical for granites of eastern Australia (Chappell *et al.*, 2012). They have a higher Fe_2O_3/FeO ratio (Figure 7), plot in the oxidised field on the Fe_2O_3/FeO *vs* Rb/Sr plot of Blevin and Chappell (1995) and exhibit lower Ba and Eu anomalies (Figure 3e, f) and hence are not fractionated. Their zircon crystals contain lower concentrations of U, Th, Ta, Nb, Y and P (Figure 4) and were likely derived from a less evolved melt (Belousova *et al.*, 2002). The hydrothermal activity generated by the magmatic episode of oxidised volcanic rocks formed white mica, chlorite and siderite alteration in the Cu deposits spatially associated with tin at the HMF.

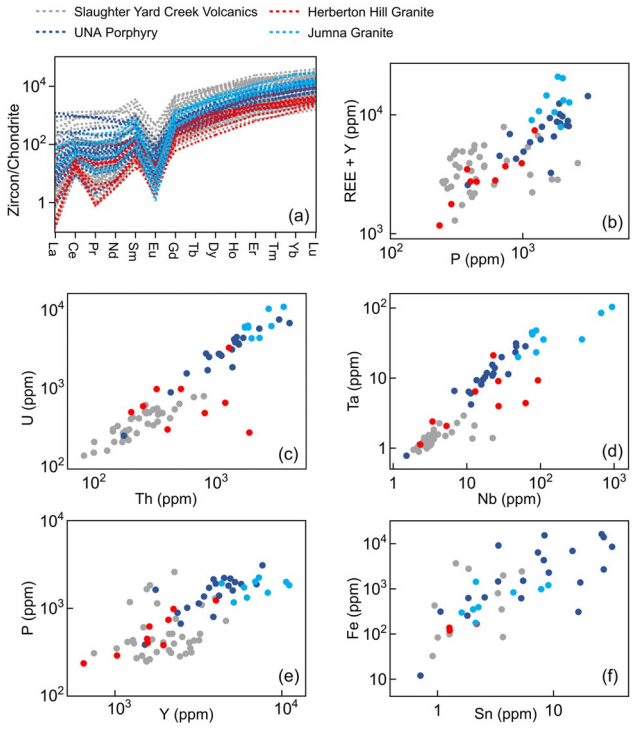

Figure 4. (a) Chondrite (values from Palme & O'Neill, 2014) normalised REE patterns for zircon. (b) REE+Y *vs* P plot. Trace-element correlation plots for (c) Th *vs* U, (d) Nb *vs* Ta, (e) P *vs* Y and (f) Sn *vs* Fe.

Muscovite trace elements as an indicator of reduced or oxidised granites

The genetic link of muscovite and topaz to host rocks, together with their trace-element geochemistry, can be used to

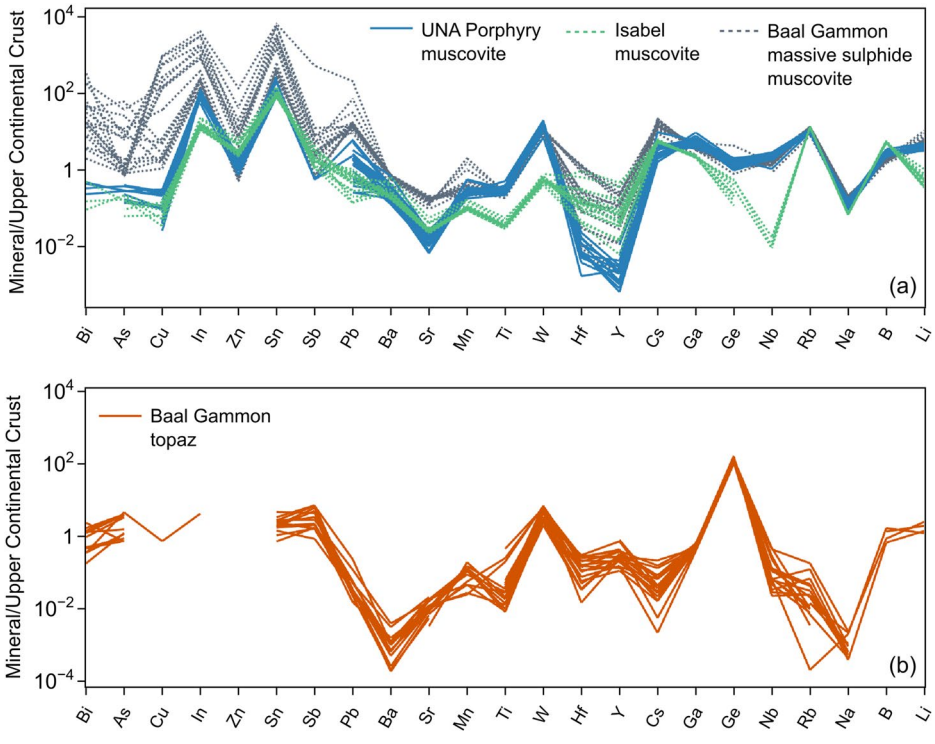

Figure 5. Upper continental crust (values from Rudnick & Gao, 2014) normalised multi-element plot of (a) mica and (b) topaz from the Baal Gammon and Isabel deposits in the HMF. The elements are plotted in order of decreasing enrichment to the left in the altered rocks.

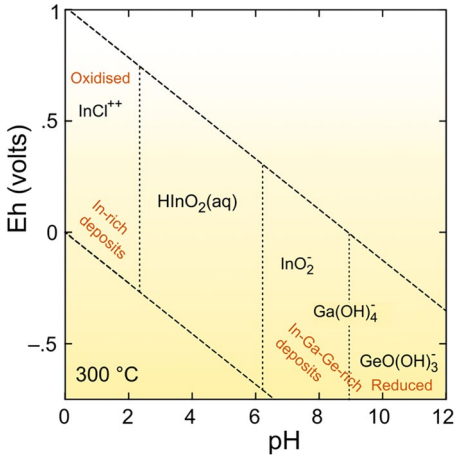

Figure 6. Eh–pH diagram for In, Ge and Ga in hydrothermal system at 300 °C developed in The Geochemist's Workbench (Bethke *et al.*, 2022) under the following conditions: $[Ga^{3+}] = 10^{-5}$, $[In^{3+}] = 10^{-5}$, $[Ge^{3+}] = 10^{-5}$, pressure = 1 bar and H_2O at unity.

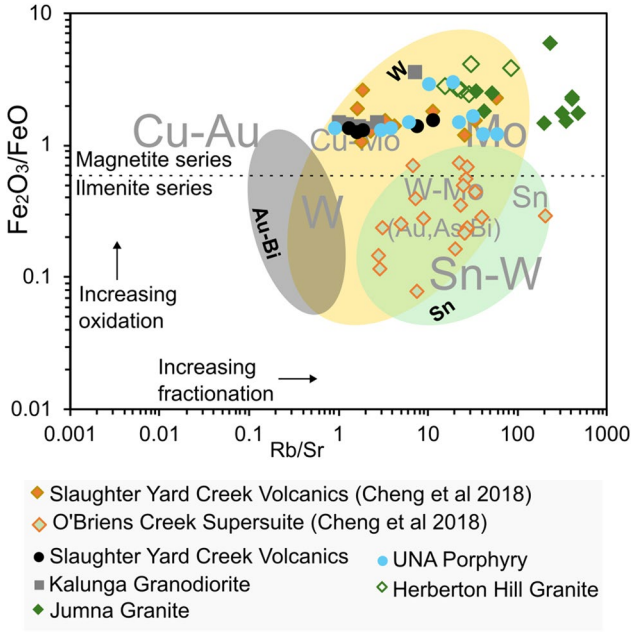

Figure 7. Oxidation and fractionation state of the HMF rock units. The Fe_2O_3/FeO *vs* Rb/Sr plot was compiled from Baker *et al.* (2005), Blevin (2004), and Blevin and Chappell (1995).

differentiate muscovite grains from reduced and oxidised granitic sources. Hydrothermal topaz at the Baal Gammon deposit occurs as an alteration product formed by the fluids generated during the emplacement of the reduced UNA Porphyry, while the muscovite grains from the Baal Gammon (Figure 2e) and Isabel deposits (Figure 1d) are the products of hydrothermal alteration that formed during sulfide mineralisation and are closely associated with the oxidised rocks of the Slaughter Yard Creek Volcanics. Similar alteration patterns were observed in other Sn–Cu deposits in the HMF (Blake & Smith, 1971). Anomalies for In, Zn, Sn, Ga and Ge were observed in the muscovite plots (Figure 5). Muscovite grains associated with the Slaughter Yard Creek Volcanics contain averages of 60 ppm In and 68 ppm Ga, whereas those from the UNA Porphyry contain an average of 5.5 ppm In and 106 ppm Ga (Table 1). This indicates that fluids associated with oxidised magmas may promote In incorporation in muscovite, whereas fluids derived from reduced intrusions favour Ga incorporation. These differences likely reflect variations in fluid pH and ligand availability rather than redox control. Another possibility for the higher In concentration in the muscovite from the Slaughter Yard Creek Volcanics could be the presence of sulfide inclusions. However, we avoided the sulfides by examining the laser profiles and selecting flat and stable signal intervals. At the Bathurst Mining Camp, Canada, In (average 48 ppm) and other trace-element (Sb, Tl and Sn) anomalies in muscovite were found as positive vectors towards massive sulfide deposits linked to oxidised rocks (Soltani Dehnavi *et al.*, 2018). The trace-element fractionation pattern of topaz (Figure 5) indicates a positive anomaly for Ga and Ge, whereas In concentrations were below the limit of detection. Topaz in the ore assemblage is representative of the magmatic–hydrothermal alteration related to the reduced Sn-granites (Lehmann, 2021). Therefore, the positive Ga anomaly in topaz further confirms its affinity for reduced magmatic–hydrothermal fluids, whereas In prefers oxidised magmatic–hydrothermal fluids (Figure 5).

The HMF muscovite geochemistry was compared with tin-related granites from the Cornubian Batholith in England (Putzolu *et al.*, 2024), the Madeira pluton in Brazil, the Kimi intrusion in Finland, the Orlovka intrusion in Russia, the Cínovec and Nejdek intrusions in the Czech Republic, the Argemela intrusions in Portugal, the Beauvoir intrusion in France (Breiter *et al.*, 2023) and the Weilasituo porphyry in NE China (Gao *et al.*, 2019). All these Sn-bearing granites are representative of the reduced granitic source rocks and were not altered by later intrusive events. The upper continental crust normalised muscovite fractionation pattern of the oxidised units of the HMF displays a strong negative anomaly for Ga and a weak negative anomaly for Ge (Figure 8). In contrast, the granites of reduced affinity, including Cornubian, Cínovec, Madeira, Moldanubicum, Orlovka, Argemela, Beauvoir, Nejdek and Weilasituo pluton, display a strong positive anomaly for Ga and a weak positive anomaly for Ge (Figure 8). This geochemical fractionation pattern of Ga and Ge in micas from reduced *vs* oxidised granites indicates their affinity for reduced fluids as opposed to oxidised fluids in magmatic–hydrothermal environments, hence confirming the observations seen from the topaz geochemistry (Figure 5b). The geochemical behaviour derived from the muscovite fractionation pattern suggests that Ga and Ge enrichment is associated with reduced intrusions, likely reflecting fluid conditions characteristic of these systems rather than redox acting as a direct control. Indium, in contrast, is enriched in the fractionation pattern (Figure 8) of micas from both oxidised and reduced granite sources. Topaz from reduced source in the HMF has limited to no In (Figure 5). Geochemical modelling suggests that the presence of In in hydrothermal fluids is favoured by acidic conditions (Kumar *et al.*, 2023). Therefore, In uptake may have been controlled not by redox but by the pH of the hydrothermal fluid. The observation from muscovite geochemistry suggests that the high Ga, Ge and In anomalies can also be used to separate reduced granitic sources from oxidised (Figure 8).

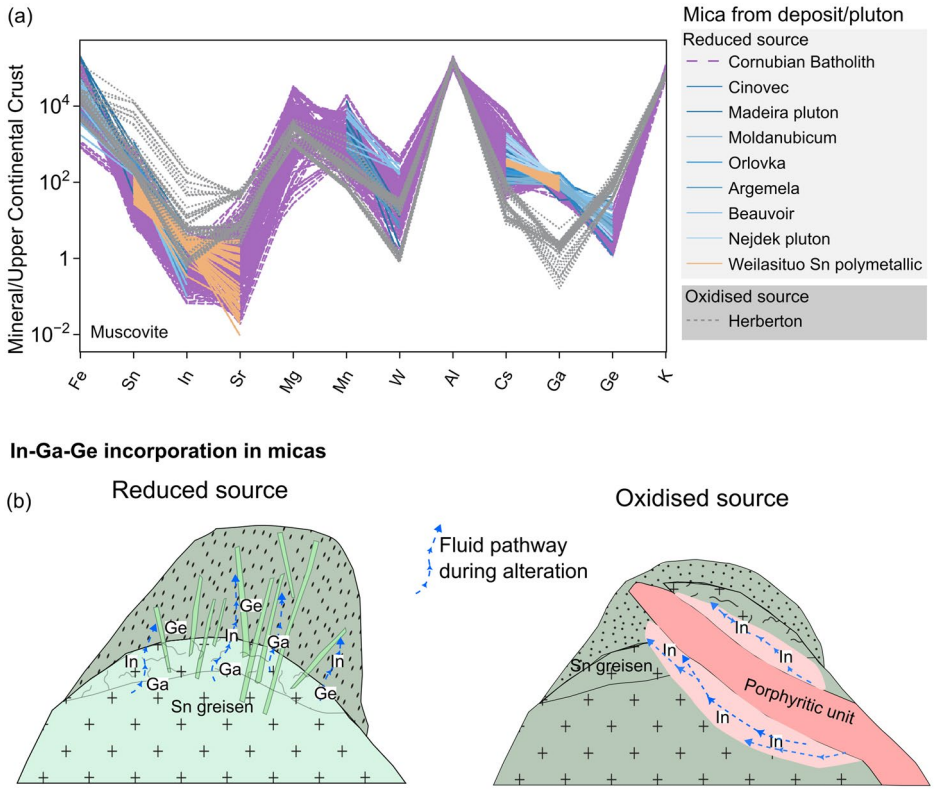

Figure 8. (a) Upper continental crust normalised muscovite geochemistry plot from the HMF in combination with literature values from Breiter *et al*. (2023), Breiter *et al*. (2023), Gao *et al*. (2019) and Putzolu *et al*. (2024). (b) Simplified greisen and porphyry model showing fluid pathways with Ga, Ge and In during alteration in reduced *vs* oxidised felsic systems.

Hydrothermal conditions for Ga, Ge and In in geochemical environments

Even though there is little information on geochemical measurement of Ga, Ge and In from natural hydrothermal systems (*e.g.* geothermal waters of New Zealand in Simmons *et al*., 2016), some inferences can be made on the geochemical behaviour of Ga, Ge and In from geochemical modelling. A temperature of 300 °C was used for modelling, since the mineralisation temperature for In-rich ores in the HMF is between 290 and 321 °C (Kumar *et al*., 2023). Similar temperature ranges, 300–400 °C, for In-rich sulfide mineralisation, were observed in other tin fields, including the Bolivian tin belt (Lehmann, 2021; Torres *et al*., 2019) and the Hämmerlein polymetallic tin deposit in Germany (Korges *et al*., 2020).

According to the modelled Eh–pH diagram (Figure 6), the speciation of In, Ge and Ga is primarily controlled by pH. Indium forms chloride complexes under acidic conditions and transitions to hydroxide and oxide complexes with increasing pH, whereas Ga is predominantly stabilised as hydroxide complexes under near-neutral to basic conditions. Redox conditions (Eh) exert a secondary control by modifying the stability fields of these species rather than acting as the primary control on speciation. Hydroxide (OH^-) group ligands form mostly in near-neutral to basic environments (White, 2020), and this limits the transportation of Ga and Ge in acidic environments. Similar In-, Ga- and Ge-ligand complexes were observed by Huston and Bastrakov (2024) for Zn-bearing deposits.

These results are reflected by the muscovite trace-element patterns from reduced and oxidised granitic sources (Figure 8a). In acidic fluids, the In–Cl complex is predominant, and with increasing pH, the hydroxide and oxide complexes are dominant (Figure 6). Conversely, Ga is predominantly present as hydroxide complexes, which are stabilised under near-neutral to basic pH conditions; in this study, these conditions are associated with reduced magmatic–hydrothermal systems. These observations are further supported by Wood and Samson (2006), whose findings indicate that In and Ga form stable complexes with hard ligands such as hydroxide, and the amphoteric nature of In allows it to form stable complexes with chlorine, which is a soft ligand. These observations are consistent with the muscovite fractionation patterns (Figure 8), where Ga and Ge enrichment is associated with reduced systems, likely reflecting fluid conditions (near-neutral to mildly basic pH and lower fO_2) that favour hydroxide complex stability. In contrast, In shows enrichment in both reduced and oxidised systems, consistent with its broader stability across a wide pH range and its sensitivity to fluid acidity. Overall, the modelling indicates that pH is the primary control on aqueous speciation of In, Ga and Ge, whereas redox conditions influence element distribution indirectly through coupling of different fluid composition and mineral equilibria.

Conclusions

In this study, the trace-element geochemistry of muscovite and topaz from the oxidised granites in the HMF was compared with reduced granites from the literature. The oxidised units in the HMF

overprinted an early Sn-greisen system (>*ca* 330 Ma) and caused chlorite alteration. The alteration assemblage associated with these granites generally contains topaz, fluorite and tourmaline. The oxidised phase of the felsic rocks at the HMF is younger (*ca* 290 Ma) and is associated with Cu deposits, with typical sericite and white muscovite alteration. The muscovite and topaz trace-element pattern allowed us to draw conclusions on the redox behaviour of Ga, Ge and In. The normalised muscovite trace-element patterns indicate that Ga and Ge show positive anomalies in reduced systems, reflecting fluid conditions associated with these environments, whereas In is less sensitive to redox and is primarily controlled by the pH of the mineralising fluid.

Acknowledgements

We thank the Economic Geology Research Centre (EGRU) at James Cook University (Townsville), and Exploration Data Centre in Brisbane, for supporting us in conducting this research.

Author contributions

Fieldwork was conducted by AAK and IS; analyses by AAK and IS; manuscript conceptualised, illustrated and written jointly by AAK, IS and MS; text edited and modified by IS and MS. All authors read and approved the final manuscript.

Disclosure statement

No potential conflict of interest was reported by the authors.

Funding

This research was funded by the Geological Survey of Queensland under the New Economy Minerals Initiative.

ORCID

A. Kumar http://orcid.org/0000-0001-7604-8949
I. Sanislav http://orcid.org/0000-0002-3680-3740
M. Sami http://orcid.org/0000-0002-0567-6283

Data availability statement

Supplementary material provided and more information can be requested at avish.kumar@jcu.edu.au.

References

Agangi, A., Gucsik, A., Nishido, H., Ninagawa, K., & Kamenetsky, V. S. (2016). Relation between cathodoluminescence and trace-element distribution of magmatic topaz from the Ary-Bulak massif, Russia. *Mineralogical Magazine*, *80*(5), 881–899. https://doi.org/10.1180/minmag.2016.080.023

Baker, T., Pollard, P. J., Mustard, R., Mark, G., & Graham, J. L. (2005). A comparison of granite-related tin, tungsten, and gold-bismuth deposits: Implications for exploration. *SEG Discovery*, *61*(61), 5–17. https://doi.org/10.5382/SEGnews.2005-61.fea

Belousova, E., Griffin, W., O'Reilly, S. Y., & Fisher, N. (2002). Igneous zircon: Trace element composition as an indicator of source rock type. *Contributions to Mineralogy and Petrology*, *143*(5), 602–622. https://doi.org/10.1007/s00410-002-0364-7

Bethke, C. M., Farrell, B., & Yeakel, S. (2022). *The Geochemist's Workbench, Version 12.0: GWB essentials guide*. LLC Champaign.

Blake, D. H. (1972). *Regional and economic geology of the Herberton/Mount Garnet area, Herberton Tinfield, North Queensland* (Vol. 124). Australian Bureau of Mineral Resources, Geology and Geophysics. https://catalogue.nla.gov.au/catalog/606297

Blake, D. H., & Smith, J. W. (1971). Mineralogical zoning in the Herberton tinfield, North Queensland, Australia. *Economic Geology*, *66*(5), 813–815. https://doi.org/10.2113/gsecongeo.66.5.813

Blanc, P., Lassin, A., Piantone, P., Azaroual, M., Jacquemet, N., Fabbri, A., & Gaucher, E. C. (2012). Thermoddem: A geochemical database focused on low temperature water/rock interactions and waste materials. *Applied Geochemistry*, *27*(10), 2107–2116. https://doi.org/10.1016/j.apgeochem.2012.06.002

Blevin, P. L. (2004). Redox and compositional parameters for Interpreting the granitoid metallogeny of eastern Australia: Implications for gold-rich ore systems. *Resource Geology*, *54*(3), 241–252. https://doi.org/10.1111/j.1751-3928.2004.tb00205.x

Blevin, P. L., & Chappell, B. W. (1995). Chemistry, origin, and evolution of mineralized granites in the Lachlan fold belt, Australia; the metallogeny of I- and S-type granites. *Economic Geology*, *90*(6), 1604–1619. https://doi.org/10.2113/gsecongeo.90.6.1604

Boschetti, T. (2023). An update on lithium mica thermodynamics and its geothermometrical application. *Geothermics*, *109*, 102661. https://doi.org/10.1016/j.geothermics.2023.102661

Breiter, K., Ďurišová, J., Korbelová, Z., Vašinová Galiová, M., & Hložková, M. (2023). Granite pluton at the Panasqueira Tungsten Deposit, Portugal: Genetic implications as revealed from new geochemical data. *Minerals*, *13*(2), 163. https://doi.org/10.3390/min13020163

Breiter, K., Gardenová, N., Vaculovič, T., & Kanický, V. (2013). Topaz as an important host for Ge in granites and greisens. *Mineralogical Magazine*, *77*(4), 403–417. https://doi.org/10.1180/minmag.2013.077.4.01

Breiter, K., Vašinová Galiová, M., Hložková, M., Korbelová, Z., Kynický, J., & Costi, H. T. (2023). Trace element composition of micas from rare-metal granites of different geochemical affiliations. *Lithos*, *446–447*, 107135. https://doi.org/10.1016/j.lithos.2023.107135

Cawood, P. A. (2005). Terra Australis Orogen: Rodinia breakup and development of the Pacific and Iapetus margins of Gondwana during the Neoproterozoic and Paleozoic. *Earth-Science Reviews*, *69*(3-4), 249–279. https://doi.org/10.1016/j.earscirev.2004.09.001

Champion, D. C. (1991). *The felsic granites of far north Queensland* [Unpublished PhD thesis]. The Australian National University.

Champion, D. C., & Chappell, B. W. (1992). Petrogenesis of felsic I-type granites: An example from northern Queensland. *Special Paper of the Geological Society of America*, *272*, 115–126. https://doi.org/10.1130/SPE272-p115

Chappell, B. W., Bryant, C. J., & Wyborn, D. (2012). Peraluminous I-type granites. *Lithos*, *153*, 142–153. https://doi.org/10.1016/j.lithos.2012.07.008

Cheng, Y., Spandler, C., Chang, Z., & Clarke, G. (2018). Volcanic–plutonic connections and metal fertility of highly evolved magma systems: A case study from the Herberton Sn–W–Mo Mineral Field, Queensland, Australia. *Earth and Planetary Science Letters*, *486*, 84–93. https://doi.org/10.1016/j.epsl.2018.01.012

Cheng, Y., Spandler, C., Kemp, A., Mao, J., Rusk, B., Hu, Y., & Blake, K. (2019). Controls on cassiterite (SnO_2) crystallization: Evidence from cathodoluminescence, trace-element chemistry, and geochronology at the Gejiu Tin District. *American Mineralogist*, *104*(1), 118–129. https://doi.org/10.2138/am-2019-6466

Codeço, M. S., Weis, P., Trumbull, R. B., Van Hinsberg, V., Pinto, F., Lecumberri-Sanchez, P., & Schleicher, A. M. (2021). The imprint of hydrothermal fluids on trace-element contents in white mica and tourmaline from the Panasqueira W–Sn–Cu deposit, Portugal. *Mineralium Deposita*, *56*(3), 481–508. https://doi.org/10.1007/s00126-020-00984-8

Dirks, H. N., Sanislav, I. V., & Abu Sharib, A. S. A. A. (2021). Continuous convergence along the paleo-Pacific margin of Australia during the Early Paleozoic: Insights from the Running River Metamorphics, NE Queensland. *Lithos*, (June), *398-399*, 106343. https://doi.org/10.1016/j.lithos.2021.106343

Duan, Z-P., Su, H-M., & Jiang, S-Y. (2024). Zircon in tin granite as tracer for fluid metasomatism and Sn mineralization. *Lithos*, *474–475*, 107597. https://doi.org/10.1016/j.lithos.2024.107597

Edgar, A., Sanislav, I., & Dirks, P. (2023). The origin of mafic–ultramafic rocks and felsic plutons along the Clarke River suture zone: Implications for porphyry exploration in the northern Tasmanides. *Australian Journal of Earth Sciences*, *70*(8), 1123–1138. https://doi.org/10.1080/08120099.2023.2234964

Edgar, A., Sanislav, I. V., & Dirks, P. H. G. M. (2022). Tectonic setting and mineralisation potential of the Cowley Ophiolite Complex, north Queensland. *Australian Journal of Earth Sciences*, *69*(8), 1132–1148. https://doi.org/10.1080/08120099.2022.2086173

Edgar, A., Sanislav, I. V., Dirks, P. H. G. M., & Spandler, C. (2022). Metamorphic diamond from the northeastern margin of Gondwana: Paradigm shifting implications for one of Earth's largest orogens. *Science Advances*, *8*(27), eabo2811. https://doi.org/10.1126/sciadv.abo2811

El Bouseily, A. M., & El Sokkary, A. A. (1975). The relation between Rb, Ba and Sr in granitic rocks. *Chemical Geology*, *16*(3), 207–219. https://doi.org/10.1016/0009-2541(75)90029-7

Eugster, H. P. (1985). Granites and hydrothermal ore deposits: A geochemical framework. *Mineralogical Magazine*, *49*(350), 7–23. https://doi.org/10.1180/minmag.1985.049.350.02

Fisher, C. M., Paton, C., Pearson, D. G., Sarkar, C., Luo, Y., Tersmette, D. B., & Chacko, T. (2017). Data reduction of Laser Ablation Split-Stream (LASS) analyses using newly developed features within iolite: With applications to Lu-Hf + U-Pb in detrital zircon and Sm-Nd + U-Pb in igneous monazite. *Geochemistry, Geophysics, Geosystems*, *18*(12), 4604–4622. https://doi.org/10.1002/2017GC007187

Fontana, D., Forte, F., Pietrantonio, M., & Pucciarmati, S. (2021). Recent developments on recycling end-of-life flat panel displays: A comprehensive review focused on indium. *Critical Reviews in Environmental Science and Technology*, *51*(5), 429–456. https://doi.org/10.1080/10643389.2020.1729073

Frenzel, M., Mikolajczak, C., Reuter, M. A., & Gutzmer, J. (2017). Quantifying the relative availability of high-tech by-product metals – The cases of gallium, germanium and indium. *Resources Policy*, *52*, 327–335. https://doi.org/10.1016/j.resourpol.2017.04.008

Gao, X., Zhou, Z., Breiter, K., Ouyang, H., & Liu, J. (2019). Ore-formation mechanism of the Weilasituo tin–polymetallic deposit, NE China: Constraints from bulk-rock and mica chemistry, He–Ar isotopes, and Re–Os dating. *Ore Geology Reviews*, *109*, 163–183. https://doi.org/10.1016/j.oregeorev.2019.04.007

Gauzzi, T., & Graça, L. M. (2018). A cathodoluminescence-assisted LA-ICP-MS study of topaz from different geological settings. *Brazilian Journal of Geology*, *48*(1), 161–176. https://doi.org/10.1590/2317-4889201820170127

Gauzzi, T., Graça, L. M., Lagoeiro, L., de Castro Mendes, I., & Queiroga, G. N. (2018). The fingerprint of imperial topaz from Ouro Preto region (Minas Gerais state, Brazil) based on cathodoluminescence properties and composition. *Mineralogical Magazine*, *82*(4), 943–960. https://doi.org/10.1180/minmag.2017.081.078

Glen, R. A. (2005). The Tasmanides of eastern Australia. *Geological Society, London, Special Publications*, *246*(1), 23–96. https://doi.org/10.1144/GSL.SP.2005.246.01.02

Henderson, R. A., Donchak, P. J. T., & Withnall, I. W. (2013). Mossman Orogen. In P. A. Jell (Ed.), *Geology of Queensland* (pp. 225–304). Geological Survey of Queensland.

Huston, D. L., & Bastrakov, E. (2024). Germanium, indium, gallium and cadmium in zinc ores: A mineral system approach. *Australian Journal of Earth Sciences*, *71*(8), 1125–1155. https://doi.org/10.1080/08120099.2024.2423772

Ishihara, S. (1981). The granitoid series and mineralization. In *Seventy-fifth anniversary volume* (pp. 458–484). Society of Economic Geologists. https://doi.org/10.5382/AV75.14

Klootwijk, C. (2013). Middle–Late Paleozoic Australia–Asia convergence and tectonic extrusion of Australia. *Gondwana Research*, *24*(1), 5–54. https://doi.org/10.1016/j.gr.2012.10.007

Korges, M., Weis, P., Lüders, V., & Laurent, O. (2020). Sequential evolution of Sn–Zn–In mineralization at the skarn-hosted Hämmerlein deposit, Erzgebirge, Germany, from fluid inclusions in ore and gangue minerals. *Mineralium Deposita*, *55*(5), 937–952. https://doi.org/10.1007/s00126-019-00905-4

Kumar, A. A., Sanislav, I. V., Cathey, H. E., & Dirks, P. H. G. M. (2023). Geochemistry of indium in magmatic–hydrothermal tin and sulfide deposits of the Herberton Mineral Field, Australia. *Mineralium Deposita*, *58*(7), 1297–1316. https://doi.org/10.1007/s00126-023-01179-7

Kumar, A. A., Sanislav, I. V., & Dirks, P. H. G. M. (2022). The geological setting of the indium-rich Baal Gammon and Isabel Sn-Cu-Zn deposits in the Herberton Mineral Field, Queensland, Australia. *Ore Geology Reviews*, *149*, 105095. https://doi.org/10.1016/j.oregeorev.2022.105095

Kumar, A. A., Sanislav, I. V., Huang, H., & Dirks, P. H. G. M. (2024). Cassiterite trace element discrimination diagrams to facilitate critical mineral exploration. *Journal of Geochemical Exploration*, *264*, 107530. https://doi.org/10.1016/j.gexplo.2024.107530

Kumar, A., Sanislav, I., Martin, L., Aleshin, M., & Dirks, P. (2024). Genesis of copper mineralization in the polymetallic tin deposits from the Herberton Mineral Field, Queensland, Australia. *Mineralium Deposita*, *59*(2), 291–311. https://doi.org/10.1007/s00126-023-01209-4

Lehmann, B. (2021). Formation of tin ore deposits: A reassessment. *Lithos*, *402-403*, 105756. https://doi.org/10.1016/j.lithos.2020.105756

Lu, F., Xiao, T., Lin, J., Ning, Z., Long, Q., Xiao, L., Huang, F., Wang, W., Xiao, Q., Lan, X., & Chen, H. (2017). Resources and extraction of gallium: A review. *Hydrometallurgy*, *174*, 105–115. https://doi.org/10.1016/j.hydromet.2017.10.010

Monnier, L., Salvi, S., Melleton, J., Lach, P., Pochon, A., Bailly, L., Béziat, D., & De Parseval, P. (2022). Mica trace-element signatures: Highlighting superimposed W-Sn mineralizations and fluid sources. *Chemical Geology*, *600*, 120866. https://doi.org/10.1016/j.chemgeo.2022.120866

Moskalyk, R. R. (2004). Review of germanium processing worldwide. *Minerals Engineering*, *17*(3), 393–402. https://doi.org/10.1016/j.mineng.2003.11.014

Palme, H., & O'Neill, H. S. C. (2014). Cosmochemical estimates of mantle composition. In H. D. Holland & K. K. Turekian (Eds.), *Treatise on geochemistry* (2nd ed., Vol. 3, pp. 1–39). Elsevier. https://doi.org/10.1016/B978-0-08-095975-7.00201-1

Paton, C., Hellstrom, J., Paul, B., Woodhead, J., & Hergt, J. (2011). Iolite: Freeware for the visualisation and processing of mass spectrometric data. *Journal of Analytical Atomic Spectrometry*, *26*(12), 2508. https://doi.org/10.1039/c1ja10172b

Peng, H-W., Yang, L-L., Lai, J-Q., Li, B., Liu, X-H., & Dai, Z-H. (2023). Mica geochemistry as an indicator of magmatic–hydrothermal processes in the Ta-Nb-Sn-W mineralization of the Limu deposit, South China. *Ore Geology Reviews*, *160*, 105584. https://doi.org/10.1016/j.oregeorev.2023.105584

Putzolu, F., Seltmann, R., Dolgopolova, A., Armstrong, R. N., Shail, R. K., Spratt, J., Buret, Y., Broderick, C., & Brownscombe, W. (2024). Influence of magmatic and magmatic–hydrothermal processes on the lithium endowment of micas in the Cornubian Batholith (SW England). *Mineralium Deposita*, *59*(6), 1067–1088. https://doi.org/10.1007/s00126-024-01248-5

Rieder, M., Cavazzini, G., D'yakonov, Y. S., Frank-Kamenetskii, V. A., Gottardi, G., Guggenheim, S., Koval', P. V., Müller, G., Neiva, A. M. R., Radoslovich, E. W., Robert, J-L., Sassi, F. P., Takeda, H., Weiss, Z., & Wones, D. R. (1999). Nomenclature of the micas. *Mineralogical Magazine*, *63*(2), 267–279. https://doi.org/10.1180/minmag.1999.063.2.13

Rosenbaum, G. (2018). The Tasmanides: Phanerozoic tectonic evolution of Eastern Australia. *Annual Review of Earth and Planetary Sciences*, *46*(1), 291–325. https://doi.org/10.1146/annurev-earth-082517-010146

Rudnick, R. L., & Gao, S. (2014). Composition of the continental crust. In H. D. Holland & K. K. Turekian (Eds.), *Treatise on geochemistry* (Vol. 4, pp. 1–51). Elsevier. https://doi.org/10.1016/B978-0-08-095975-7.00301-6

Setkova, T. V., Balitsky, V. S., Spivak, A. V., Kuzmin, A. V., Borovikova, E. Y., Kvas, P. S., Balitskaya, L. V., Nekrasov, A. N., Zakharchenko, E. S., & Pushcharovsky, D. Y. (2024). Crystal Growth, composition, structure, and Raman spectroscopy of novel Ga,Ge-rich topaz. *Journal of Crystal Growth*, *637-638*, 127723. https://doi.org/10.1016/j.jcrysgro.2024.127723

Seward, T. M., Williams-Jones, A. E., & Migdisov, A. A. (2014). The chemistry of metal transport and deposition by ore-forming hydrothermal fluids. In H. D. Holland & K. K. Turekian (Eds.), *Treatise on geochemistry* (2nd ed., Vol. 13, pp. 29–57). Elsevier. https://doi.org/10.1016/B978-0-08-095975-7.01102-5

Shand, S. J. (1948). Eruptive rocks: Their genesis, composition, classification, and their relation to ore deposits, with a chapter on meteorites. *Journal of Geology*, *56*(6), 593.

Sillitoe, R. H., & Lehmann, B. (2022). Copper-rich tin deposits. *Mineralium Deposita*, *57*(1), 1–11. https://doi.org/10.1007/s00126-021-01078-9

Simmons, S. F., Brown, K. L., & Tutolo, B. M. (2016). Hydrothermal transport of Ag, Au, Cu, Pb, Te, Zn, and other metals and metalloids in New Zealand geothermal systems: Spatial patterns, fluid-mineral equilibria, and implications for epithermal mineralization. *Economic Geology*, *111*(3), 589–618. https://doi.org/10.2113/econgeo.111.3.589

Soltani Dehnavi, A., Lentz, D. R., McFarlane, C. R. M., & Walker, J. A. (2018). Quantification of fluid-mobile elements in white mica by LA-ICP-MS: From chemical composition to a potential micro-chemical vectoring tool in VMS exploration. *Journal of Geochemical Exploration*, *188*, 290–307. https://doi.org/10.1016/j.gexplo.2018.01.017

Soufi, M. (2021). Origin and physical-chemical control of topaz crystallization in felsic igneous rocks: Contrasted effect of temperature on its OH–F substitution. *Earth-Science Reviews*, *213*, 103467. https://doi.org/10.1016/j.earscirev.2020.103467

Torres, B., Melgarejo, J-C., Torró, L., Camprubí, A., Castillo-Oliver, M., Artiaga, D., Campeny, M., Tauler, E., Jiménez-Franco, A., Alfonso, P., & Arce-Burgoa, O. (2019). The Poopó polymetallic epithermal deposit, Bolivia: Mineralogy, genetic constraints, and distribution of critical elements. *Minerals*, *9*(8), 472. https://doi.org/10.3390/min9080472

Uribe-Mogollon, C., & Maher, K. (2018). White mica geochemistry of the Copper Cliff porphyry Cu deposit: Insights from a vectoring tool applied to exploration. *Economic Geology*, *113*(6), 1269–1295. https://doi.org/10.5382/econgeo.2018.4591

van Ryt, M. R., Sanislav, I. V., Dirks, P. H. G. M., Huizenga, J. M., Mturi, M. I., & Kolling, S. L. (2019). Biotite chemistry and the role of halogens in Archaean greenstone hosted gold deposits: A case study from Geita Gold Mine, Tanzania. *Ore Geology Reviews*, *111*, 102982. https://doi.org/10.1016/j.oregeorev.2019.102982

Watari, T., Nansai, K., & Nakajima, K. (2020). Review of critical metal dynamics to 2050 for 48 elements. *Resources, Conservation and Recycling*, *155*, 104669. https://doi.org/10.1016/j.resconrec.2019.104669

Whalen, J. B., Currie, K. L., & Chappell, B. W. (1987). A-type granites: Geochemical characteristics, discrimination and petrogenesis. *Contributions to Mineralogy and Petrology*, *95*(4), 407–419. https://doi.org/10.1007/BF00402202

White, W. M. (2020). *Geochemistry*. John Wiley & Sons.

Withnall, I. W., & Henderson, R. A. (2012). Accretion on the long-lived continental margin of northeastern Australia. *Episodes*, *35*(1), 166–176. https://doi.org/10.18814/epiiugs/2012/v35i1/016

Wood, S. A., & Samson, I. M. (2006). The aqueous geochemistry of gallium, germanium, indium and scandium. *Ore Geology Reviews*, *28*(1), 57–102. https://doi.org/10.1016/j.oregeorev.2003.06.002

Zhang, L., Jiang, S., Bagas, L., Han, N., Liu, Y., & Liu, Y. (2019). Element behaviour during interaction of magma and fluid: A case study of Chamuhan Granite, and implications on the genesis of W – Mo mineralisation. *Lithos*, *342-343*, 31–44. https://doi.org/10.1016/j.lithos.2019.05.025

Zheng, K., Benedetti, M. F., & van Hullebusch, E. D. (2023). Recovery technologies for indium, gallium, and germanium from end-of-life products (electronic waste) – A review. *Journal of Environmental Management*, *347*, 119043. https://doi.org/10.1016/j.jenvman.2023.119043